Accurate Atomic Mass Measurements from Penning Trap Mass Comparisons of Individual Ions

F. DiFilippo, V. Natarajan†, M. Bradley, F. Palmer, and D.E. Pritchard

Research Laboratory of Electronics, Department of Physics, Massachusetts Institute of Technology, Cambridge, MA 02139, USA and †AT&T Bell Laboratories, Murray Hill, NJ 07974 USA.

Abstract. We report measurements of mass ratios of 20 pairs of molecular ions with a single ion Penning trap mass spectrometer having an accuracy exceeding one part in 10^{10}. The dominant source of error is random magnetic field fluctuations which cause a 2.6×10^{-10} rms scatter in measurements of the cyclotron frequency. Robust statistical analysis of the data ensures that nongaussian outliers are weighted less heavily in a smooth and consistent manner. Systematic errors are estimated to be 2×10^{-11} or below for doublet mass comparisons. The ratios form an overdetermined set, such that the atomic masses of nine isotopes can be derived from at least two independent groups of ion mass ratios, providing many consistency checks for systematic errors at the 10^{-10} level. At this level of precision, certain mass measurements have important implications in fundamental metrology. Results presented here are essential for defining a practical atomic standard of mass, for calibrating γ-ray wavelengths, and for determining the molar Planck constant and the fine structure constant.

1. INTRODUCTION

The precision at which mass comparisons can be made has steadily improved over the years. Recently, the Penning trap has emerged as the most accurate instrument for mass spectrometry. A precision exceeding 10^{-10} is routinely attained in our experiment at MIT (1). The major purpose of this paper is to present accurate measurements of twenty different mass ratios that determine ten atomic masses and to present a thorough analysis of the uncertainties in these measurements. We also describe several new metrological implications of our mass comparisons.

The basic advantages of a Penning trap for mass measurement are that the mass is determined from a frequency measurement, that a long time is available to make this measurement, and that the ion is confined to a small spatial region of a highly uniform magnetic field. A Penning trap consists of a strong magnetic field $\vec{B}$ (providing radial confinement) and a weak quadrupole electric field $\vec{E}$ (providing axial confinement) (2). In order to eliminate coulombic perturbations due to other nearby ions and uncertainties due to unspecified internal motion of a cloud of trapped ions, we perform measurements on a single trapped ion.

The physics of a single ion in a Penning trap is well understood and has been described in detail in the literature (3). The motion is a superposition of three normal modes of oscillation: the "axial" mode, the "trap cyclotron" mode, and the "magnetron" mode. The axial mode is harmonic oscillation along the magnetic field lines at a frequency ω_z that is proportional to the square root of the trap voltage. The trap cyclotron mode (at ω_c') is similar to ordinary cyclotron motion in the radial plane, with the frequency slightly perturbed by the electric field. The magnetron mode (at ω_m) is a much slower circular motion essentially due to $\vec{E} \times \vec{B}$ drift. The "free-space" cyclotron frequency ω_c, which would be the frequency of cyclotron motion if the electric field were removed, is obtained by adding the three mode frequencies in quadrature:

$$\omega_c = \left(\omega_c'^2 + \omega_z^2 + \omega_m^2\right)^{1/2} = \frac{qB}{mc} \ , \qquad (1)$$

where q and m are the charge and mass of the ion (in CGS units), and c is the speed of light. In our trap, B = 85000 G, and for an N_2^+ ion (mass 28 u, where u ≡ atomic mass units), the mode frequencies ω_c', ω_z, and ω_m are 4.6 MHz, 160 kHz, and 2.8 kHz, respectively. Therefore, only the trap cyclotron frequency ω_c' must be measured to the desired precision of ω_c.

For optimum precision, the frequency, phase and amplitude of the ion's axial motion must be accurately extracted from the smallest possible signal. The ion's axial motion is observed by detecting the image current (~10^{-14} A) induced in the endcaps of the trap. A high-Q (~30,000) superconducting tuned circuit and an rf SQUID are used to attain a sufficient signal-to-noise ratio (4). The axial signal is a sinusoid that decays as the ion loses its energy into the detector. This signal is analysed by pre-multiplying the data with exp(-t/τ), where τ is the amplitude decay time, and then taking a fourier transform. The ion's parameters are obtained by finding the peak of the transform. This procedure works better than a simple digital Fourier transform because it weights the data taken at later times progressively less (5). We have shown (6) that this procedure gives unbiased estimates and gives errors that are close to theoretical minimum bounds for a given signal to noise ratio.

The radial modes are observed and cooled indirectly by coupling them to the axial mode with a diagonally oriented quadrupole rf field (7). The advantage of this scheme is that the cyclotron mode is not damped by the detector (thus having a nearly zero linewidth) and also does not experience tuned circuit pulling. However, an indirect approach must be taken to measure ω_c'.

We have developed two such approaches to determine ω_c': the "*p*ulse a*n*d *p*hase" (PNP) method and the "*s*eparated *o*scillatory *f*ields" (SOF) method. Both methods utilize "π-pulses" of the diagonal rf field at $\omega_c' - \omega_z$ to coherently exchange the amplitudes (scaled by $\omega^{1/2}$) and phases of the axial and trap cyclotron modes, allowing the amplitude and phase of the trap cyclotron mode to be determined (8). With the PNP method, the trap cyclotron frequency is measured by exciting the ion to a cyclotron amplitude ρ_c, allowing the ion to evolve "in the dark" for a delay time *T*, and applying a π-pulse to measure the accumulated phase (9). With the SOF method(10), the ion is excited by a pair of cyclotron pulses separated by a delay time *T*, so that the final cyclotron amplitude varies sinusoidally with the phase accumulated between the pulses. The amplitude is then measured by a π-pulse. The SOF method is well suited for measurements of non doublets since the cyclotron motion of both ions can be studied with the same electric fields, with the trap voltage then being changed just before the π-pulse in order to bring the axial frequency into resonance with the detector. With both methods, ω_c' is measured to 10^{-10} precision with a series of measurements, the longest having a delay time of ~1 minute, so that proper phase unwrapping is achieved. Related techniques are used to cool the magnetron motion so that the ion is located at the center of the trap before measuring ω_c'.

2. DETERMINING A MASS RATIO

If the magnetic field were known as a function of time, a mass ratio of two different ion species could be determined by comparing the free-space cyclotron frequencies for two ions, measured at times t_1 and t_2,

$$\frac{m_1}{m_2} = \frac{q_1}{q_2}\frac{B(t_1)}{B(t_2)}\frac{\omega_{c2}(t_2)}{\omega_{c1}(t_1)}\ , \qquad (2)$$

since the ratio q_1/q_2 is a known rational number, and the ratio ω_{c2}/ω_{c1} is measured to high precision. Unfortunately, the magnetic field drifts unpredictably in the time between and during two measurements and does not cancel exactly. The field can change by processes internal or external to the magnet, the major source during the day being external magnetic fields from a nearby subway. Motion of the trap relative to the magnet may also change the field at the trap center because of field gradients. Although other sources of random error (such as trap voltage fluctuation and thermal noise) contribute to temporal variations in repeated measurements of the cyclotron frequency, the magnetic field fluctuations dominate (see section 5). We therefore model all temporal variation of ω_c as if the magnetic field were the only contributor.

Fitting to field drift

In order to account for the effects of temporal drift, measurements are repeated while alternating between the two species being compared. A plot of the cyclotron frequency data for a typical run is shown in Fig. 1. With this scheme, ω_c is measured for each ion at several different times, allowing the drift to be

determined. However, the field drift can be determined and corrected for only if it occurs on a time scale longer than the time between measurements of different ions, which is typically 10-20 minutes. Short-term field fluctuations cannot be modeled, and they contribute to the uncertainty in the mass ratio. The time dependence of the magnetic field can be written as:

$$B(t) = B(0)\left(1 + f(t) + \delta B(t)\right) , \tag{3}$$

where $f(t)$ is the modeled long-term field drift and $\delta B(t)$ is the unknown short-term field behavior.

The mass ratio is obtained by fitting to the data for both ions simultaneously. If the fitting is done by the least squares method, then the quantity

$$\sum_j \left(\omega_{c1}(t_j) - f(t_j) - \Delta\omega_c\right)^2 \Big/ \sigma_j{}^2 \; + \; \sum_k \left(r_0\,\omega_{c2}(t_k) - f(t_k)\right)^2 \Big/ \sigma_k{}^2 \tag{4}$$

is minimized with respect to the fitting function $f(t)$ and the frequency difference between the two curves $\Delta\omega_c$. Here, the indices j and k indicate individual

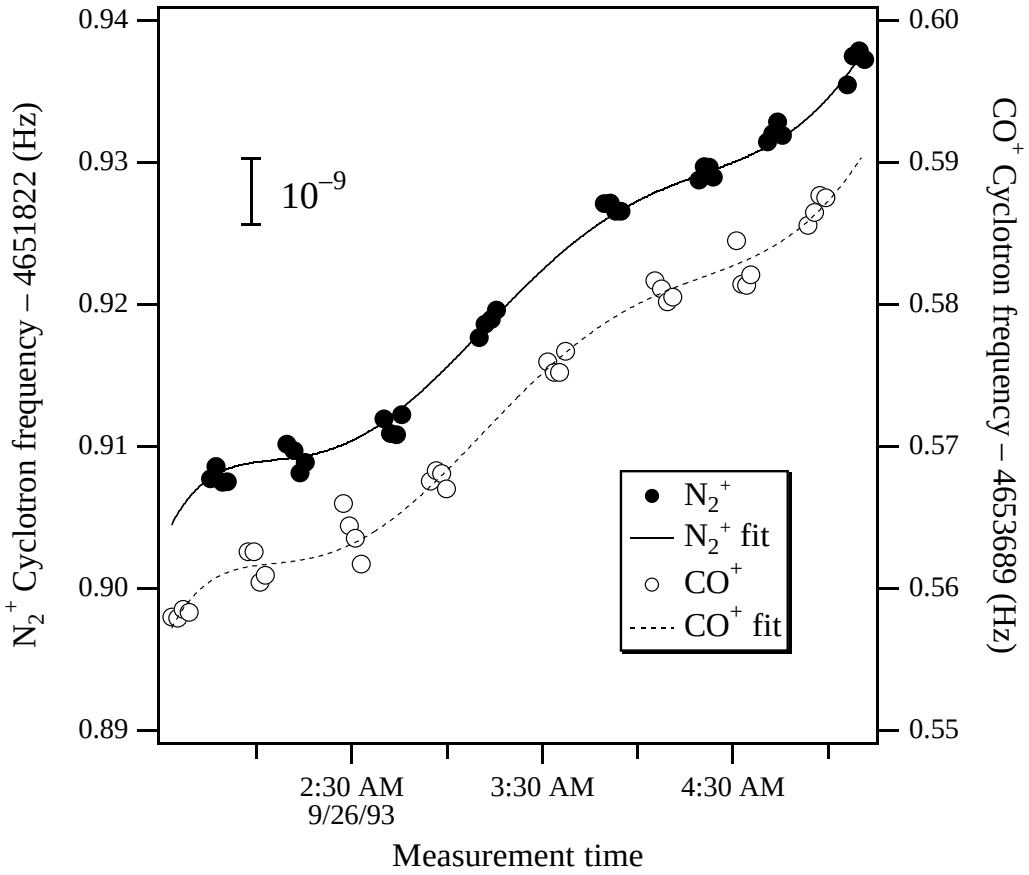

Figure 1. Typical data for an ion mass ratio measurement. The cyclotron frequency is measured alternately for the two ions in order to fit to the field drift and to determine the mass ratio.

measurements for the two ions, r_0 is an initial guess of the mass ratio (obtained from existing atomic mass data), and σ is the measurement uncertainty. For a doublet (a pair of ions of nominally the same mass, such as N_2^+ and CO^+), $r_0 \cong 1$. The best value of the frequency difference,

$$\Delta\omega_c = \omega_{c1}(0) - r_0\,\omega_{c2}(0) \tag{5}$$

leads directly to the mass ratio *r*,

$$r \;=\; \frac{m_2}{m_1} \;=\; r_0 + \frac{\Delta\omega_c}{\omega_{c1}(0)} \tag{6}$$

The uncertainty in *r* arises from the short-term field fluctuations $\delta B(t)$ and will be discussed in the next section.

The simplest general functional form to use for $f(t)$ is a polynomial. The order of the polynomial is critical. If too few terms are used, the polynomial may not fit the drift adequately. Conversely, if too many terms are used, the polynomial may exaggerate short-term fluctuations, giving unreliable results. Thus there is an optimal order of polynomial to use for a data set.

The data reported here were taken over a period exceeding one year, and the roughly equal earlier and later portions were analyzed in two significantly different ways. For the earlier portion (6) we used our best judgement to determine the order of the polynomials, and used conventional least squares fitting algorithms. For the latter portion (11) we used a more conservative statistical test to determine the number of polynomials, and a modification of least square statistics called "robust" statistics which provides improved handling of points (called "outliers" henceforth) that deviate from the mean by several standard deviations.

For the more recent portion of the data, the basis for deciding whether the next higher-order term should be added to the polynomial is whether it produces a significant statistical improvement in the fit. Goodness of fit is characterized by the χ^2 statistic (the quantity minimized in Equation (4)):

$$\chi_n^2 = \sum_{i=1}^{N} \left(\Delta_i/\sigma_i\right)^2 \;, \tag{7}$$

where Δ is the deviation from the fit, σ is the measurement uncertainty, *n* is the order of the polynomial fit, and *N* is the total number of points for both ions. Improvement in the fit due to an additional term (the *F*-test) (12) is characterized by the relative change in χ_n^2:

$$F_\chi(n) \;=\; \frac{\chi_{n-1}^2 - \chi_n^2}{\chi_n^2/\nu} \;, \tag{8}$$

where ν is the number of available degrees of freedom (to be discussed shortly). Assuming purely random fluctuations, the quantity F_χ follows the *F* distribution, since it is a ratio of χ^2 statistics. The probability *P* that the term of order *n* is statistically significant can be determined from tables of F_χ *vs* ν (12). (By coincidence, a probability of 0.5 corresponds to a value of $F_\chi \sim 0.5$ for low orders of *n*.) Our procedure is to increase the order of the polynomial until two

consecutive fits give $P < 0.5$ (because the field may accidently have no variation corresponding to a particular order). The optimal order is chosen to be the last one having $P > 0.5$.

In most statistical analyses, the number of degrees of freedom ν is taken to be $N - n - 1$, the number of data points minus the number of terms in the fit (n plus a constant term). This assumes that the data points are all uncorrelated, which is not true in our case, since points within a "cluster" (a group of successive measurements on the same ion – see Fig. 1) are more strongly correlated. We adopted a more conservative estimate for ν:

$$\nu = N^* - n - 2 \ , \tag{9}$$

where N^* is the number of clusters in the data set. (The "2" arises from the fact that $\Delta\omega_c$ is an extra parameter in the fit.) This ensures that only long-term drift affecting more than one cluster is considered and prevents the polynomial from fitting to field jumps on a time scale smaller than the time between clusters. Thus, for example, a minimum of five clusters is needed for a quadratic ($n = 2$) fit.

Figure 2 illustrates the dependence of χ^2, F_χ, and the calculated mass ratio on the order of the polynomial fit, for the CO^+/N_2^+ measurement illustrated in Fig. 1. Fig. 2a shows that χ^2 decreases quickly at first and later stabilizes as the order is increased. In Fig. 2b, F_χ is plotted along with a dotted line corresponding to $P = 0.5$, showing that $n = 6$ is the optimal order in this case. As seen in Fig. 2c, the calculated mass ratio did not vary much, although variations on the order of 1 σ have been observed in other measurements for small n.

A result of this conservative treatment of the number of degrees of freedom has been that some measurements needed to be discarded. For certain runs (apparently when the magnet's liquid helium level was low), the magnetic field was exceedingly erratic. Polynomials whose order approached the number of clusters of data seemed to be necessary in order to fit to the field fluctuations, indicating significant field variation on the time scale required to change ions. The above definition for ν does not allow such a high-order fit, and we decided to discard such data completely. These data included our earlier measurement of the $^{14}N/CH_2^+$ ratio (13), which was 1.5 sigma higher than the value of this ratio determined from our more recent measurements of $^{14}N_2/C_2H_4^+$.

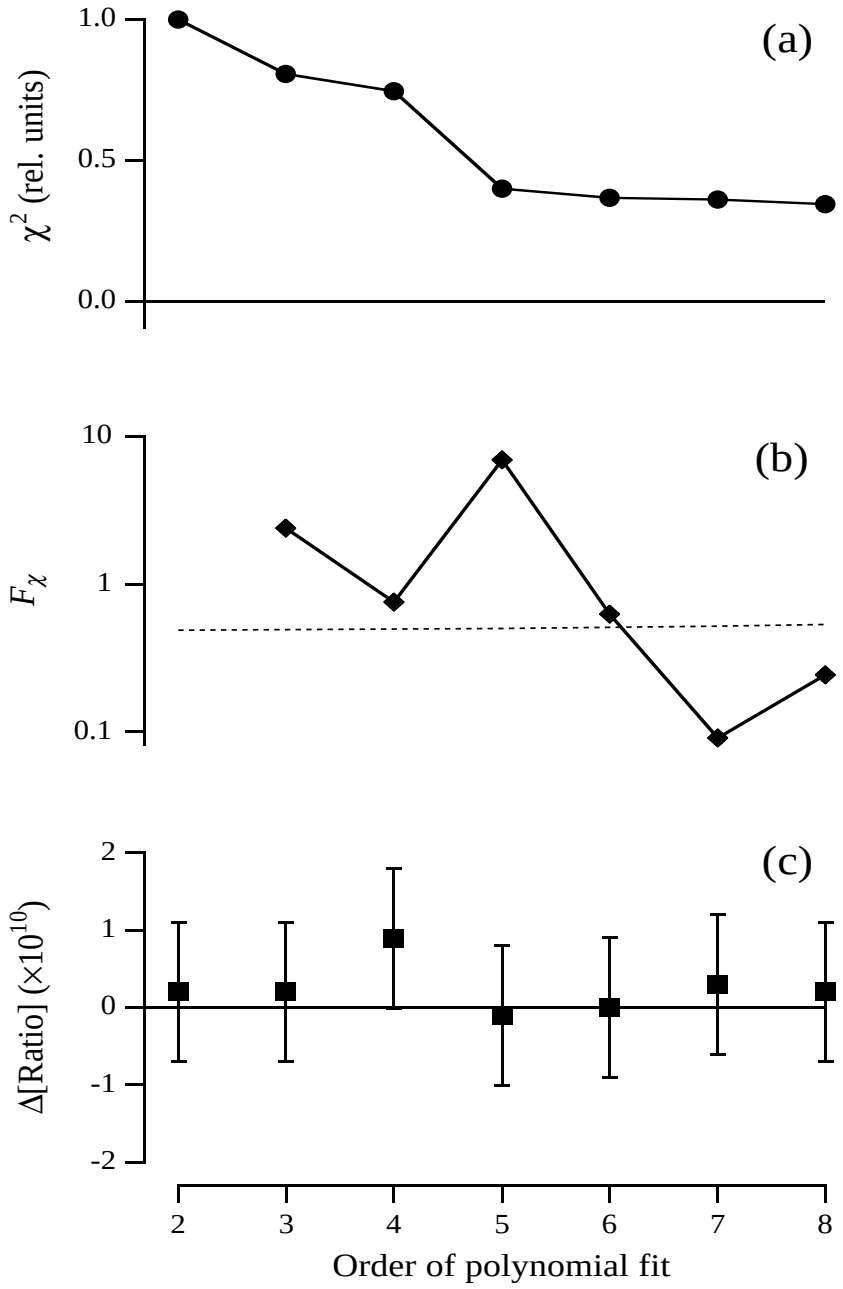

Figure 2. Choosing the order of the polynomial fit. The χ^2 statistic (a), the F_χ statistic (b), and the calculated mass ratio (c) are plotted as a function of the order of the polynomial *n* for the data in Fig. 1. The dotted line in (b) indicates the value of F_χ corresponding to a 50% statistical probability that the observed value would be exceeded if the data were normally distributed. (Note that it increases slightly with *n*.) In this case, a 6th order polynomial was determined to be optimal.

3. MAGNETIC FIELD NOISE

The above procedure describes how we model long-term field drift and extract the mass ratio from the data. The unknown component of Equation (3), the short-term field fluctuation $\delta B(t)$, appears as scatter about the fit and leads to uncertainty in the mass ratio. This field noise is the dominant source of error in our experiment, and its statistics must be well understood. A detailed analysis of the magnetic field noise and its effect on mass ratios is presented in this section. Other sources of error, both random and systematic, are considered in the next section and shown to be insignificant.

Traditional statistics is based on the assumption that random variables follow the normal (gaussian) distribution. This assumption often does not apply to real experiments, where some of the fluctuations may be due to a less frequent but more intense external noise source, or where the fluctuations may not be normally distributed ($1/f$ noise for example). A qualitative model of such an observed noise distribution P is a superposition of a dominant gaussian component P_G along with a small component P_N that is much wider: (14)

$$P = (1-\varepsilon)P_G + \varepsilon P_N \tag{10}$$

where $\varepsilon \ll 1$. The effect of P_N is to increase the probability of observing a large fluctuation. Although a gaussian distribution predicts that variations larger than 3σ should only occur 0.3% of the time, they occur much more often in most real experiments. Thus, P is a nearly gaussian distribution for small variations, but with tails that approach zero more slowly.

The magnetic field noise distribution $P(\delta B)$ for all the data in the second part of our experiment has been observed to follow this model. Experimentally, $P(\delta B)$ is measured by compiling a histogram of deviations from curve fits to the data from many runs. The histogram shown in Fig. 3a consists of about 1000 measurements and appears to be gaussian near the center with standard deviation $\sigma = 2.6\times10^{-10}$. When the histogram is plotted on a semi-logarithmic scale (Fig. 3b), the gaussian central portion of the distribution is parabolic, and the extra outliers are readily apparent.

These excess outliers can have adverse effects on data analysis, especially if the least squares method from traditional statistics is used. Since the goal is to minimize the sum of squares of the deviations from the fit, outliers are heavily weighted and could significantly pull the mean. Data rejection methods exist which attempt to identify and eliminate non-gaussian outliers, but these methods have been shown to be biased for varying degrees of noise contamination (14).

Robust statistical analysis

Our approach has been to use robust statistics (14), which maintains the least squares philosophy while accounting for outliers in a smooth and consistent manner. A class of robust statistics called "*M*-estimates" is a generalization of least squares statistics and is easily implemented in nonlinear regression. Near the center, a robust distribution approximates a gaussian distribution.

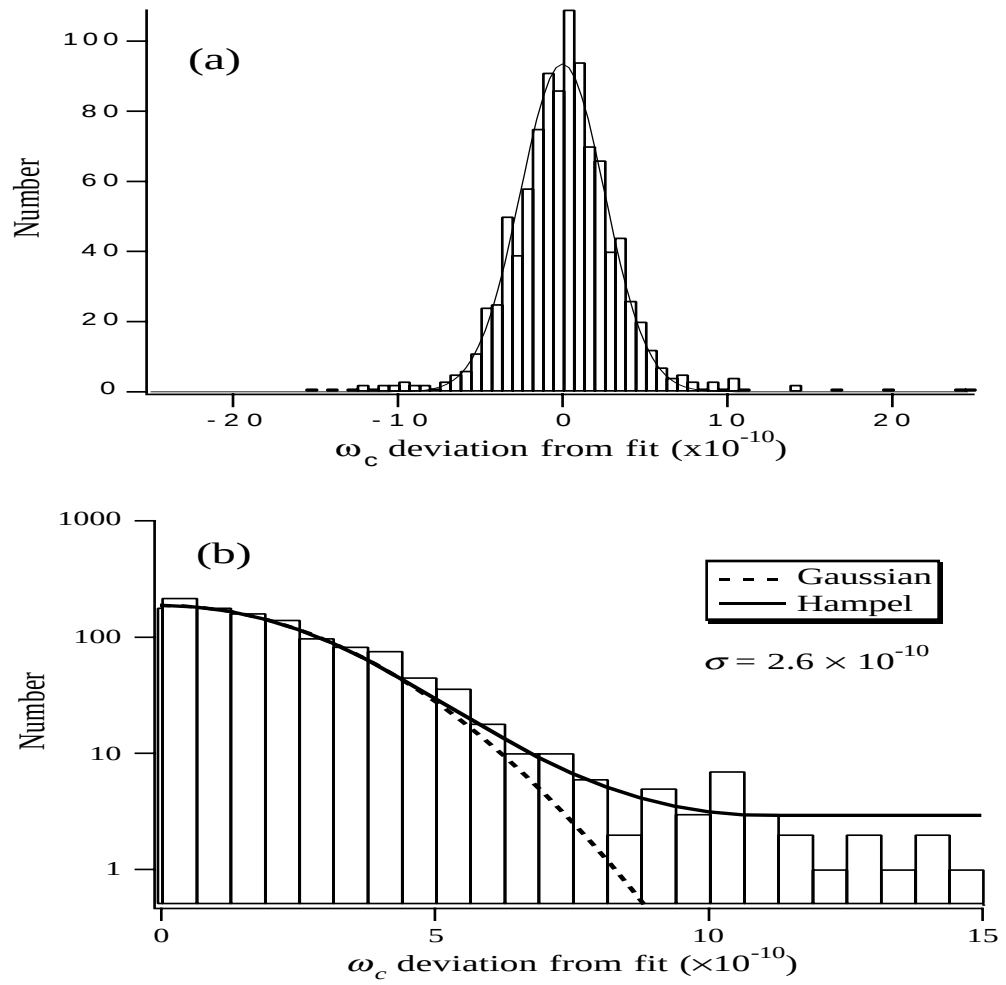

Figure 3. Cyclotron frequency noise. In (a), a histogram of the differences between the measured ω_c's and the fit to the field drift is plotted for ~1000 measurements, along with a gaussian fit with s = 2.6 x10^{-10}. The excess number of outliers is apparent in (b), where the histogram is folded and plotted on a logarithmic scale. The distribution corresponding to the Hampel estimator in Fig. 4 represents the observed noise more accurately than the conventional gaussian (least-squares) distribution.

Data with larger deviations from the fit Δ are weighted less, and the corresponding probability distribution $P(\Delta)$ has larger tails than a gaussian to account for extra outliers. This distribution can be expressed in terms of an "estimator" $\psi(\Delta)$:

$$P(\Delta) = \exp\left(-\int_0^{\Delta} \psi(\Delta')\, d\Delta'\right) \tag{11}$$

Since the maximum likelihood estimates of the fit parameters are obtained by solving $\sum_i \psi(\Delta_i) = 0$, the estimator $\psi(\Delta)$ is proportional to the effect of a data

point with deviation Δ on the fit. The least squares case is given by $\psi(\Delta) = \Delta$, in which all data points are weighted evenly and affect the fit in linear proportion to their deviation from the fit, and the probability distribution is the familiar gaussian: $P(\Delta) = \exp(-\Delta^2/2)$. A robust estimator, on the other hand, has $\psi(\Delta) = \Delta$ for points with small deviations (where gaussian statistics is valid) and $\psi(\Delta) < \Delta$ for points with large deviations (thus diminishing the importance of the outliers).

We use a three-part descending Hampel estimator $\psi(x)$ (Fig. 4) to fit to the field noise. (Many statisticians consider this estimator to be well representative of actual physical data (15).)

$$\psi(x) = \begin{cases} x & \text{for } |x| < a \\ a\ \mathrm{sgn}(x) & \text{for } a < |x| < b \\ a(c-|x|)/(c-b) & \text{for } b < |x| < c \\ 0 & \text{for } |x| > c \end{cases}, \tag{12}$$

where $x = \Delta/\sigma$, and where a, b, and c are parameters, chosen to be 1.6, 2.5, and 4.3, respectively. These parameter values were selected to accurately reflect the observed probability distribution in Fig. 3. Points with deviations larger than $a\sigma$ have reduced weight, and those with deviations larger than $c\sigma$ are completely rejected from the fit (*i.e.*, $\psi \to 0$). Although only six points were seen outside the range of Fig. 3(b), others may have been missed because their phase error exceeded π, resulting in misassignment of the phase or in rejection of that datum due to uncertainty in unwrapping the phase.

Fitting with robust statistics is equivalent to performing a weighted least squares fit (14). The assigned error in each measurement is weighted by a factor of $w = \psi(\Delta)/\Delta$. Points with small Δ thus receive full consideration by the fit

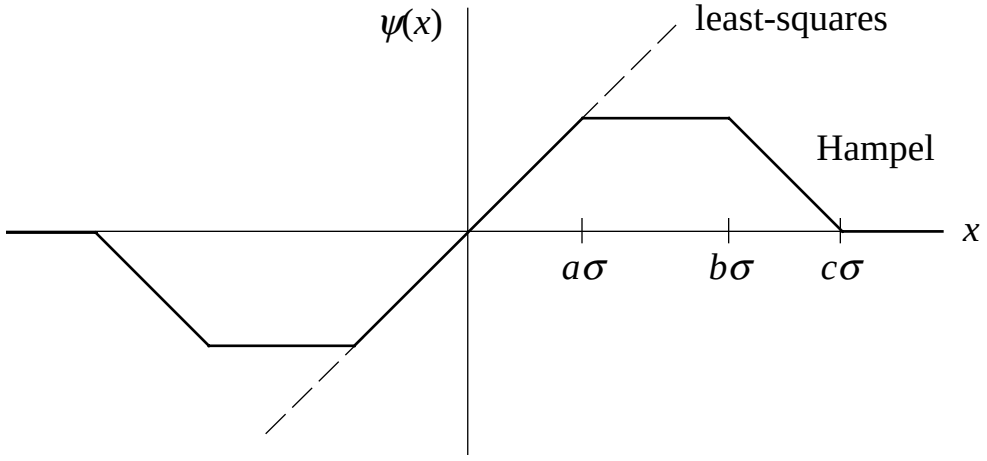

Figure 4. Hampel estimator. The three-part descending Hampel estimator (12) used for modeling fluctuations in ω_c (Fig. 3) is shown, along with the conventional least-squares estimator. Points with large deviations ($> a\sigma$) are weighted less and have a smaller effect on fitting to field drift.

($w = 1$), and points with large Δ receive reduced consideration ($w < 1$). Least squares fitting is done iteratively (since Δ changes after each attempt) until the fit parameters converge. The resultant uncertainty in the difference frequency $\Delta\omega_c$ is the standard statistical error (from χ^2 curvature) from assigning an uncertainty of $2.6\times10^{-10}\,/\,w$ to each point. For a nighttime run, the statistical uncertainty in $\Delta\omega_c$ and therefore in the associated mass ratio is typically 1×10^{-10}.

Ultimately, the use of robust statistics has made relatively little difference in our final results. When robust and standard techniques were applied to the same data, the results were usually within $\sigma/2$ of each other. The standard deviations observed in the later set of runs were generally close to 2.6×10^{-10} whereas standard deviations of the earlier set of runs occasionally were as high as 4×10^{-10}. We believe this is primarily due to better shimming of the field (so that movement of the trap vacuum system in its dewar does not affect the results so much, but it results partly from the fact that the robust statistics deweight the outliers somewhat. As described below (see Consistency checks), comparisons of final results from the two different sets of runs showed no statistically significant deviations.

4. ATOMIC MASSES

Mass ratios were measured for a wide variety of molecular ions, and the results are listed in Table 1. The ion species were selected so that atomic masses of the neutral isotopes could be determined in terms of $m[^{12}\mathrm{C}]$, the basis of the atomic mass scale. In this section, the procedure for converting the ratios into atomic masses is described.

The first step in converting ion mass ratios into masses of neutral atoms in the ground state is to account for chemical binding energies and ionization energies:

$$m[\mathrm{A_nB_k}^+] = m[n\mathrm{A}_{(g)} + k\mathrm{B}_{(g)} - e^-] + \Delta E/c^2 \tag{13}$$

The energy ΔE required to form a molecular ion from the neutral atoms is calculated from the standard heats of formation of the species in the gaseous state at 0 K temperature (16). Afterwards, the mass ratio r can be expressed in terms of the individual atomic masses, as in this example:

$$r = \frac{m[\mathrm{A}_n\mathrm{B}_k^+]}{m[\mathrm{C}_p\mathrm{D}_q^+]} = \frac{m[n\mathrm{A} + k\mathrm{B} - e^-] + \Delta E_1/c^2}{m[p\mathrm{C} + q\mathrm{D} - e^-] + \Delta E_2/c^2} \tag{14}$$

For doublet measurements, $(1-r) \sim O(10^{-3})$, and the mass ratio should be considered as a determination of a mass difference:

$$m[p\mathrm{C} + q\mathrm{D} - n\mathrm{A} - k\mathrm{B}] = (1-r)\Big(m[p\mathrm{C} + q\mathrm{D} - e^-]\Big) + \Delta E'/c^2 \tag{15}$$

Table 1. Measured mass ratios and corresponding mass differences (in atomic mass units). The numbers in parentheses indicate the uncertainty in the last decimal places. Several ratio measurements were repeated in order to reduce statistical error.

Ratio	Value	Runs	Difference	Value [u]
$N_2^+ / C_2H_4^+$	0.999 102 696 201 (55)	4	C + 2H – N	0.012 576 059 8 (8)
$^{15}N_2^+ /$	0.998 547 569 780 (50)	4	C + D + H - ^{15}N	0.021 817 911 9 (8)
CO^+ / N_2^+	0.999 598 887 572 (77)	3	2N – C – O	0.011 233 390 9 (22)
$CO^+ / C_2H_4^+$	0.998 701 943 805 (66)	2	C + 4H – O	0.036 385 507 3 (19)
$^{13}C_2H_4^+ /$	0.999 805 486 870 (77)	2	C + D - ^{13}C - H	0.002 921 908 6 (12)
Ar^{++} / Ne^+	0.999 437 341 275 (106)	2	2Ne – Ar	0.022 497 224 5 (42)
$Ar^+ / C_3H_4^+$	0.998 278 399 350 (88)	2	3C + 4H – Ar	0.068 917 005 3 (35)
$CD_3^+ / CD_2H_2^+$	0.999 914 190 780 (100)	2	2H – D	0.001 548 283 6 (18)
Ne^+ / CD_4^+	0.996 810 562 610 (130)	1	C + 4D – Ne	0.063 966 932 9 (26)
Ar^{++} / CD_4^+	0.996 249 698 100 (100)	1	2C + 8D – Ar	0.150 431 104 5 (40)
CD_4^+ / C^+	1.671 397 950 390 (310)	1	D	2.014 101 778 5 (9)
CD_3^+ / C^+	1.503 548 462 350 (200)	1	D	2.014 101 777 6 (6)
Ar^+ / Ne^+	1.998 902 121 050 (300)	1	2Ne - Ar	0.0224972276 (60)
O^+ / CH_4^+	0.997 730 269 420 (80)	1	C + 4H – O	0.036 385 506 2 (13)
CH_4^+ / C^+	1.335 957 033 780 (230)	1	H	1.007 825 031 7 (7)
$SiH_2^+ /$	0.998 293 230 200 (80)	1	2C + 2D – Si	0.051 277 022 4 (24)
$SiH_2^+ / {}^{15}N_2^+$	0.999 745 290 400 (80)	1	2^{15}N – Si – 2H	0.007 641 200 7 (24)
$^{15}N^+ / CH_3^+$	0.998 444 631 990 (110)	1	C + 3H – ^{15}N	0.023 366 197 9 (17)
$CO_2^+ / C_3H_8^+$	0.998 348 443 160 (100)	1	C + 4H – O	0.036 385 506 0 (22)
$^{13}CH_4^+ /$	0.999 828 496 650 (90)	1	C + D - ^{13}C - H	0.002 921 907 4 (15)

Although C and D also appear on the right side of the equation, they are multiplied by the small factor $(1-r)$ and do not need to be known *a priori* to high precision. Note that species which appear in both the numerator and the denominator cancel to first order in the mass difference. (For example, the ratio $m[CD_3^+]/m[CD_2H_2^+]$ determines the mass difference $2H - D$.)

The mass differences and their uncertainties, also listed in Table 1, can be expressed in matrix form:

$$x\,M = y \pm \sigma \tag{16}$$

where x is a $P \times Q$ matrix of the coefficients, M is a column vector of the Q atomic masses, and $y \pm \sigma$ is a column vector of the P mass differences and uncertainties. (The reference atom ^{12}C, which is defined to have a mass of exactly 12 u, is included on the right side of the equation.) The best values of the atomic masses are obtained from a global least squares fit:

$$M = X^{-1}Y \tag{17}$$

where

$$X_{jk} = \sum_{i=1}^{P} x_{ij}x_{ik}/\sigma_i^2 \quad , \quad Y_j = \sum_{i=1}^{P} x_{ij}y_i/\sigma_i^2 \tag{18}$$

The inverted matrix X^{-1} is the covariance matrix, the diagonal elements of which are the uncertainties in the atomic masses.

The ability to invert the X matrix depends on whether each individual species can be directly related to ^{12}C. This is rather difficult to accomplish solely with doublets in the mass range in which we operate (10-50 u). (For example, the three ratios N^+/CH_2^+, O^+/CH_4^+, and CO^+/N_2^+ would seem sufficient to determine the atomic masses of N, O, and H, but the resultant matrix is singular; *i.e.*, the mass differences from these ratios using (15) are linearly dependent.) We have measured one set of doublets ($Ar^+/C_3H_4^+$, Ar^{++}/CD_4^+, and $CD_3^+/CD_2H_2^+$) which determines H and D directly in terms of C and breaks the singularity in the matrix. We have also developed techniques to make non-doublet measurements (10), such as CH_4^+/C^+, which are very useful for providing links to invert the matrix.

Atomic mass table

An atomic mass table (Table 2) of nine isotopes and the neutron is obtained by fitting to the entire set of our mass ratio measurements. For comparison, the best values from conventional mass spectrometry (the 1983 atomic mass evaluation (17)) are also listed, showing that Penning trap measurments have achieved an improvement in precision of a factor of 10-1000. The latest (1993) atomic mass evaluation (13) contains some data from Penning trap experiments, including preliminary values of some results reported here. Our latest results are consistent with our earlier (6) results , except for the 1.5 σ adjustment in the ^{14}N mass that followed the new data analysis described previously (section two).

The neutron mass follows from the atomic masses of ^1H, ^2H, and the deuteron binding energy from:

$$^1H + n \rightarrow {}^2H + \gamma \quad (2.2\ \text{MeV}) \ , \tag{19}$$

The most accurate measurement of the γ-ray wavelength (18) is accurate to 1×10^{-6} and limits the precision of our determination of the neutron mass to 2×10^{-9}.

Other Penning trap measurements

Table 2 also compares our measurements with other Penning trap experiments. The results are in good agreement with our more precise values, except for a two sigma difference for ^{16}O. Van Dyck *et. al.* (19) have written a detailed review of high precision mass measurements in Penning traps. Their group has measured the masses of several light isotopes (19), most notably ^3He and ^3H (20), with uncertainties typically a factor of 2 larger than ours. They use a trap similar to ours, but having a small anharmonicity such that the axial frequency is a weak function of the cyclotron amplitude.

Table 2a. Atomic mass table. The masses (in u) of nine isotopes and the neutron are listed as determined from this experiment, from the 1983 atomic mass evaluation [15], and from other single-ion Penning trap experiments [17,19]. The numbers in parentheses indicate the error in the rightmost figures. The uncertainty in the neutron mass from this experiment is limited by the error in the deuteron binding energy [16].

Species	Mass (this work)	Non-Penning trap values [15]	Other Penning trap values
1			
2			
13			
14			
15			
16			
20			
28			
40			

Table 2b. Atomic mass differences measured by the MIT Penning trap experiment and the Ohio State FT-ICR experiment.

Mass difference	MIT value [u]	Ohio State value [u]
$CH^+ - N^+$	0.012 576 046 4 (6)	0.012 576 039 0 (190) [20]
$H_2O^+ - DO^+$	0.001 548 279 4 (9)	0.001 548 296 0 (120) [21]
$D_2O^+ - {}^{20}Ne^+$	0.030 677 980 2 (25)	0.030 677 480 0 (670) [22]

Measurements are made by monitoring the axial frequency while a drive is swept through the (trap) cyclotron frequency. They have solved the matrix inversion problem by measuring q/m doublets containing highly ionized species such as $^{12}C^{3+}$ and $^{4}He^{+}$. The Stockholm-Mainz group has measured the mass of ^{28}Si with 10^{-9} precision (21). Their technique is similar to one used for unstable nuclei (22). Ions are ejected from the trap through a hole in the endcap. As they leave the magnetic field, their cyclotron energy is converted to additional axial velocity, which is monitored by time of flight. Fourier transform ion cyclotrometers are widely used in analytical and physical chemistry. (23) These devices have a ring that is divided into four quadrants, with two quadrants used to excite the cyclotron motion and two used for detection. The group at Ohio State has determined several mass differences by FT-ICR spectrometry on ion clouds with uncertainties about 20 times larger than our corresponding values (24-26).

5. UNCERTAINTIES

In the previous discussion, it was assumed that random field fluctuations dominated the uncertainty in the experiment. There are several other sources of error below 10^{-10} that prove negligible but still should be considered. In this section, the various uncertainties, both random and systematic, are summarized and estimated. In Table 3, the uncertainties contributed from the various sources are listed for a single measurement of ω_c as well as for a measurement of the mass ratio during a nighttime run. For the purpose of calculation, errors are estimated for a typical ion of mass 30 u; Table 3 also lists how each error scales with the mass of the ion being measured.

Random errors

The observed noise histogram in Fig. 3 is a composite of all short-term fluctuations which contribute to the random error of the experiment. The rms error is 2.6×10^{-10} per measurement of ω_c, and the resultant error in the mass ratio is typically 1×10^{-10} for a nighttime run of ~60 measurements with ~15 alternations of the ions. Variations in the magnetic field at the site of the ion (from both internal and external processes) are primarily responsible for this random error.

Electric field fluctuations also contribute to the random error, but to a lesser extent. The axial frequency ω_z varies as the square root of the trap voltage, which is subject to electrical noise and drift. Since the trap cyclotron frequency ω_c' is measured over a ~1 min integration time, and ω_z is measured immediately afterwards, the trap voltage fluctuations do not cancel in Equation (1) and appear as random fluctuations in ω_c. The shot-to-shot variation in ω_z due to trap voltage instability has been observed to be ~10 mHz. For an ion of mass 30 u, this corresponds to a 9×10^{-11} error in ω_c per shot, resulting in a 3×10^{-11} random error in the mass ratio from a typical run.

Thermal noise in the cyclotron amplitude also causes random error in ω_c. Since the ion is cooled by a resistive detector, there is thermal uncertainty in the ion's initial location in phase space. The axial temperature T_z has been measured to be ~10 K, which is slightly higher than the 4 K liquid He bath because of additional noise from the rf SQUID detector. The cyclotron mode is thermally coupled to the axial mode using sideband cooling (7), resulting in a cyclotron temperature T_c equal to $T_z\left(\omega_c'/\omega_z\right)$, which is ~300 K for a mass 30 u ion, corresponding to a thermal rms amplitude of 0.0015 cm. During a measurement, this thermal amplitude adds vectorially to a mean amplitude of typically 0.025 cm from the applied cyclotron excitation pulse, causing variations in the cyclotron amplitude ρ_c from measurement to measurement.

Due to anharmonicities from relativity and higher-order field imperfections, these variations in ρ_c lead to variations in the measured cyclotron frequency ω_c. To lowest order (3),

$$\Delta\left(\frac{\delta\omega_c}{\omega_c}\right) = \left(-\frac{{\omega_c}^2}{2c^2} - \frac{B_2}{2B_0} + \frac{3\omega_m C_4}{2\omega_c d^2}\right)\Delta\left({\rho_c}^2\right) \qquad (20)$$

Table 3. Summary of estimated random [R] and systematic [S] uncertainties for doublet (d) and non-doublet (n) comparisons, in parts per trillion (10^{-12}). The first column lists the error contributed from each source per measurement of the cyclotron frequency ω_c, and the second column lists the resultant error in the mass ratio for a single nighttime run. Errors are calculated for mass 30 u ions, assuming a cyclotron amplitude $\rho_c = 0.025$ cm, a magnetic bottle $B_2/B_0 < 10^{-6}$ cm^{-2}, and a higher-order electric field $C_4 < 10^{-4}$, among other assumptions described in the text. The last column indicates how each uncertainty scales with the mass m of the ion.

Source of uncertainty	Error in ω_c (ppt)	Error in ratio (ppt)	Scaling
Magnetic field fluctuations	260 [R]	100 [R]	—
Electric field fluctuations	90 [R]	30 [R]	$(m/30)^2$
Thermal noise	30 [R]	10 [R]	$(30/m)^{3/2}$
Spectral estimation (w)	90 [R]	30 [R]	$m/30$
Spectral estimation (phase)	100 [R]	30 [R]	—
r imbalance (relativity)	10(d), 20(n) [S]	10(d), 20(n) [S]	$30/m$
r imbalance (B)	10(d), 30(n) [S]	10(d), 30(n) [S]	$m/30$
r imbalance (C)	9(d), 30(n) [S]	9(d), 30(n) [R]	$(m/30)^3$
C imbalance	20 [S]	20 [R]	$30/m$
Surface patch charges	4(d), 0(n) [S]	4(d), 0(n) [S]	$30/m$
Trap tilt (magnetron)	0(d), 40(n) [S]	0(d), 40(n) [S]	$(m/30)^4$
Tuned circuit pulling	2 [S]	2 [R]	$m/30$

where B_2/B_0 is the magnetic bottle, C_4 is the fourth-order electric field coefficient, and $d^2 = 0.3$ cm^2 is the characteristic trap size. We have made the field flaws B_2/B_0 and C_4 smaller than 10^{-6} cm^{-2} and 2×10^{-4}, respectively, by adjusting the magnet's shim coils and the trap's guard ring electrodes. After shimming, the relativistic correction is the dominant term, particularly for light ions. Therefore thermal noise, in conjunction with these anharmonicities, causes a random error of 3×10^{-11} per run for a mass 30 u ion and 1.6×10^{-10} per run for a mass 10 u ion. Although this error is insignificant now, it may be dominant in two-ion mass spectrometry (27), in which both magnetic and electric field fluctuations cancel. We have proposed classical squeezing methods able to reduce the effects of thermal noise by about a factor of 5 (28). Recently, we have demonstrated the ability to squeeze the thermal noise and to reduce amplitude fluctuations by parametric amplification at $2\omega_z$ (29).

Another source of random error is detector noise, limiting the ability to extract frequency and phase information from the detected signal. The axial frequency ω_z can be determined to ~10 mHz. This adds to the random error in the same way as trap voltage fluctuations, contributing an uncertainty of 9×10^{-11} in a typical mass ratio. The phase of the ion's axial motion can be determined to ~10 degrees, out

of a total phase which is accumulated over an integration time T of typically 1 minute. For a mass 30 u ion, this phase error contributes an uncertainty of $\sim 1\times10^{-10}$ per measurement of ω_c. This error depends inversely on T, and T is chosen long enough so that the magnetic field fluctuations are dominant.

Systematic errors

The anharmonicities in Equation (20) could also lead to systematic errors in the mass ratio. Since ω_c is measured with a nonzero cyclotron amplitude ($\rho_c \sim 0.02$ cm), nonlinear terms cause a frequency shift of $\sim 10^{-9}$. For doublets, this shift cancels to lowest order since the ions are pulsed to nearly the same amplitude. However, a systematic imbalance in ρ_c would cause a systematic error in the mass ratio. One source of imbalance in ρ_c is the transfer function of the cyclotron drive electronics. The transfer function was characterized from the Rabi frequencies of π-pulses, and the upper limit for ρ_c imbalance was found to be 2% (11). This limit leads to upper bounds on systematic error of 1×10^{-11} from both relativity and the magnetic bottle B_2. The error from the higher-order electric field C_4 in conjunction with an imbalance in ρ_c is below 2×10^{-11}.

An imbalance in ρ_c becomes an axial amplitude imbalance after the π-pulses, causing different shifts in the axial frequencies if C_4 is not zero. If the gross anharmonic shift in axial frequencies is 0.1 Hz, a 40 mHz difference will occur between the two axial frequency shifts, causing an error of 6×10^{-11} in the heaviest ratios we have measured, but for most ratios the error is closer to 2×10^{-11}.

It is also possible to have an imbalance in C_4 between the two ions, if the trap is tuned differently for each. Assuming a 50 μV difference in the scaled guard ring potential, the resultant error in the mass ratio would be 2×10^{-11}. (This estimate is based on an experimentally observed shift of 8×10^{-10} for a mass 40 u ion with a 2.4 mV offset (6).) This error is only significant for measurements on heavy ions (>20 u), for which the present apparatus requires that the guard ring potentials be set manually for both ions. (In an earlier measurement of the CO^+/N_2^+ ratio, the guard ring potentials were set improperly, and a 2×10^{-10} correction subsequently had to be made in the ratio reported in (30).) Although the errors involving C_4 are systematic over the course of one run, they are random for ratio measurements on different nights because the trap is retuned (changing C_4) before each run.

For non-doublets, these anharmonic shifts do not cancel to lowest order. Instead, the cyclotron amplitudes are controlled so that the relativistic shifts cancel, and corrections are made for the B_2 and C_4 shifts (10). The resultant systematic errors are calculated to be $\sim 6\times10^{-11}$, small compared to the random error from field noise.

Image charges moving in the electrodes at the cyclotron frequency lower that frequency by about 50 microhertz per charge. This has negligable effect on doublet measurements, but measurements of different charge states and non-doublet measurements can be shifted by at most 2×10^{-11}.

Other sources of error contribute at the 10^{-12} level. Surface charge patches on the trap electrodes cause a shift in the ion's equilibrium position, which is different for the two ions because the trap voltage is different. Because of magnetic field gradients, the two ions experience different fields, causing a systematic error of 4×10^{-12} for doublets. (Surface patches would not cause such an error in non-

doublet measurements, since the two ions are measured with the same trap voltage (10).)

The magnetron frequency ω_m is not measured during the run; it does not need to be known very accurately, since the effect of an error in ω_m is scaled down by a factor of $(\omega_m/\omega_c)^2$. In an ideal trap, ω_m can be determined from $\omega_z^2/2\omega_c'$; however this relation is perturbed by a factor of $\left(1+(9/4)\sin^2\theta\right)$ when the trap is tilted with an angle θ with respect to the magnetic field (3). The magnetron frequency is measured once per run by observing the avoided crossing with an rf coupling drive (8) to determine the trap tilt (0.66(2)°, in our case), so that ω_m can be deduced from subsequent measurements of ω_z and ω_c'. The correction factor $(9/4)\sin^2\theta$ can be determined to about 5%. The resultant error for a doublet measurement is completely negligible — a few parts in 10^{14}. For non-doublets, the error is a few parts in 10^{11}, still considerably smaller than the random error.

Tuned circuit pulling also is a potential cause of systematic error. Since the ion's axial mode is coupled to a high-*Q* tuned circuit, ω_z is perturbed. Assuming an unlikely systematic difference of 50 mHz in the two ions' axial frequencies during one run, the resultant uncertainty in ω_c is 2×10^{-12}.

In summary, the magnetic field noise causes a random error of $\sim10^{-10}$ in one mass ratio run, and other sources of random and systematic errors are calculated to be about an order of magnitude smaller. In the next section, it is shown that the quoted uncertainties are verified by a series of checks.

Consistency Checks

In a precision experiment, the reported uncertainty is just as important as the reported result, and there is a need to check for unknown errors to ensure that none have been overlooked. The fact that we measure mass ratios of molecular ions, which involve various combinations of atomic species, affords an opportunity for self-consistent checks of systematic and random errors. We have done many such checks to ensure that our uncertainties are accurate. These checks may be classed in several categories: repeated measurements, closed loops of ratios, repeated measurements after a complete reshimming of our magnet, redundant ratios, non-doublet measurements, and the overall agreement of the global fit to all ratios.

Repeated measurements. In many cases, measurements were repeated on the same pair of ions on several nighttime runs. The field fluctuations typically were different for each run, therefore testing the method of fitting to the field drift. There were 13 repeated measurements, having a reduced chi-square of $\chi_\nu^2 = 0.75$. This test indicates that the random error from field fluctuations, as determined by the histogram in Fig. 3, has not been underestimated.

Closed loops. Another check involves "closed loops" of ratios. Given three ions A^+, B^+, and C^+, there are three possible doublets that can be measured: A^+/B^+, B^+/C^+, and C^+/A^+. If the ratios are multiplied together, the product should be equal to one, within experimental error. Closed loops are basically a check on the field fitting uncertainties, like repeated measurements, except that they are also sensitive to any systematic errors which are nonlinear with respect to the

difference in mass. Three such closed loops were measured, having a reduced chi-square of $\chi^2_\nu = 1.53$. (Statistically, a reduced chi-square of this value or higher should arise in 20% of the cases, so $\chi^2_\nu = 1.53$ is not anomalously high.)

Magnet reshimming. In the midst of our measurements, our superconducting magnet accidentally quenched. This divided the data into "earlier" and "later" categories which were analysed differently as discussed in sections 2 and 3. The magnet was rebuilt, reenergized, and reshimmed, changing the higher-order inhomogeneities in the magnetic field. In this process, the trap was thermally cycled between 300 K and 4 K, changing the surface patch charges on the trap electrodes which contribute to higher-order terms in the electric field. Comparison of measurements done before and after the magnet rebuild therefore checks systematic errors resulting from field imperfections. There were three such measurements, having a reduced chi-square of $\chi^2_\nu = 0.26$.

Redundant ratios. A particularly powerful check for systematics is provided by redundant ratios, measurements that determine the same mass difference using different molecular ions. For example, the ratios O^+/CH_4^+, $CO^+/C_2H_4^+$, and $CO_2^+/C_3H_8^+$ all determine the mass difference $C + 4H - O$, but the measurements are made at mass 16, 28, and 44 u, respectively. Such redundant ratios check for virtually all systematic errors, since the ratios are measured under widely different experimental conditions. For example, different trap voltages test for errors from surface patch charge effects, different cyclotron frequencies test for errors in the phase-coherent cyclotron mode coupling techniques, and different chemical energies test for errors in the method of calculating atomic masses from ratio measurements. The ratios that were measured contain a total of four redundancies with $\chi^2_\nu = 0.39$.

Non-doublet ratios. We have developed techniques (10) to measure ratios of non-doublets, which are pairs of ions with greatly different mass. Non-doublet ratios were compared with measurements of doublet ratios, providing a test of possible systematic errors arising from differences in the measurement techniques. Anharmonic frequency shifts which cancel to lowest order for doublets do not

Table 4. Summary of consistency checks. The number of excess independent measurements ν and the reduced chi-square χ^2_ν are listed. The last column lists the statistical probability P of exceeding the observed value of χ^2_ν for each check.

Check	ν	χ^2_ν	P
Repeated measurements	13	0.75	71%
Closed loops	3	1.53	20%
Magnet rebuild	3	0.26	85%
Redundant ratios	4	0.39	82%
Doublet / non-doublet	3	0.16	92%
Overall	24	0.74	81%

naturally cancel for non-doublets. The cyclotron modes are intentionally driven to different amplitudes in order to cancel the relativistic shift, but a magnetic bottle shift remains. Three doublet / non-doublet redundancies resulted in $\chi_\nu^2 = 0.16$, indicating that such systematic errors are insignificant at the 10^{-10} level of precision.

An additional test of the non-doublet comparison method is by the measurement of the known ratios N_2^+/N^+ and Ar^+/Ar^{++} (10). In each case, the ratio is about equal to two, except for corrections from the electron mass and the chemical energies. Since N and Ar are compared against themselves, their atomic masses with respect to C cancel to lowest order, and the ratios can be calculated from existing mass data with an accuracy of $\sim 10^{-12}$. The measured ratios were found to agree with the calculated values, adding further confidence to our non-doublet measurement technique.

Overall agreement. The final consistency check is the overall agreement of all the results in the global least squares fit. There are a total of 33 ratio measurements and 9 atomic masses, and therefore 24 degrees of freedom. The reduced chi-square for the fit was $\chi_\nu^2 = 0.74$. Table 4 lists all the reduced chi-squares from the different types of checks, as well as the statistical probability for exceeding the observed value of χ_ν^2. In all cases, $\chi_\nu^2 \sim 1$, and the reported uncertainties can be considered to be consistent with the data. These consistency checks therefore are compelling evidence that the errors in the mass ratios are dominated by the observed statistical noise. The checks also imply that if any systematic error had been overlooked, it would have to be smaller than 10^{-10}.

Every isotope in our mass table is derived from at least two independent sets of ratios (except for the neutron, which depends on a single gamma-ray experiment). This not only provides the same checks as the redundant ratios described above, but also ensures that non-canceling calculational and measurement errors have been avoided.

6. APPLICATIONS TO METROLOGY

At the 10^{-10} level of precision, certain mass measurements have important implications for fundamental metrology (1). In this section, we discuss the contributions of our measurements to defining an atom-based mass standard, calibrating γ-ray wavelengths, and determining fundamental constants.

Atomic mass standard

Our demonstrated ability to compare atomic masses at the 10^{-10} level establishes comparison of atomic masses as a more precise operation than comparison of macroscopic masses, which is limited to a relative precision of $\sim 10^{-9}$, especially for masses of different density (31). This suggests the wisdom of an atomic definition of mass, as might be achieved by defining the Avogadro constant, N_A. Finding an accurate way to realize such a definition would have the additional advantage of replacing the last artifact standard, the kilogram.

The S.I. unit of mass, the kilogram, is defined to be the mass of the prototype platinum-iridium cylinder at Bureau International des Poids et Measures. Besides being unique, such an artifact mass standard has many disadvantages, including the possibility of long-term drift and damage due to mishandling (31). (To guard against mishandling, the prototype kilogram has been compared to secondary

standards only three times this century.) A more desirable standard would be based on an atomic mass, such as the mass of a ^{28}Si atom, which avoids these disadvantages (32). However, replacing the artifact mass standard depends on the ability to realize the kilogram (*i.e.*, to develop a practical macroscopic mass standard from this atomic definition).

One promising method for realizing an atomic kilogram is to accurately measure the lattice constant and the mass density of a highly-pure silicon crystal (33). With the present mass standard, this experiment determines the Avogadro constant N_A; with an atomic mass standard based on a defined value of N_A, the crystal becomes a mass density standard which would lead to a macroscopic realization of the kilogram. A precision in N_A of 1×10^{-6} has been attained so far (33), and it is anticipated that modifications (including the use of a crystal isotopically enriched with ^{28}Si) will allow N_A to be measured to 10^{-8} in the future. (Recently, a measurement of the silicon lattice constant d_{220} has been reported to 3×10^{-8} (34).) Realizing the kilogram with 10^{-8} accuracy would at the very least provide a check on the long-term drift of the artifact mass standard. The previous (non-Penning-trap) value of $M(^{28}\mathrm{Si})$ was accurate to 2.5×10^{-8} and would have been a limitation in the accuracy of N_A. The value from our experiment, accurate to 7×10^{-11} and confirmed to 10^{-9} (21), removes this limitation.

γ-ray calibration

Another application of precision mass spectrometry in the field of metrology is to "weigh" γ-rays. By Einstein's principle, $\Delta E = \Delta m c^2$, the energy released in a nuclear process in the form of γ-rays can be measured as a difference in the mass of the initial and final nuclei. If the γ-ray energy is in the form of a single photon with effective wavelength λ^*, after correcting for nuclear recoil, then the energy balance equation is:

$$E_\gamma = hc/\lambda^* = \Delta m c^2 \tag{21}$$

Absolute measurements of γ-ray wavelengths are often imprecise. For this reason, neutron separation energies determined by mass spectrometry are used to calibrate γ-ray wavelengths, particularly in the 2-13 MeV range (35).

The neutron capture reactions ^{14}N(n, γ) and ^{12}C(n, γ) are two processes that are attractive for γ-ray wavelength calibration:

$$\begin{aligned} {}^{14}\mathrm{N} + n &\rightarrow {}^{15}\mathrm{N} + \gamma_1 + \gamma_2 \quad (10.8\ \mathrm{MeV}) \\ {}^{12}\mathrm{C} + n &\rightarrow {}^{13}\mathrm{C} + \gamma \quad (4.9\ \mathrm{MeV}) \end{aligned} \tag{22}$$

When combined with ^{1}H(n, γ):

$$ {}^{1}\mathrm{H} + n \rightarrow {}^{2}\mathrm{H} + \gamma \quad (2.2\ \mathrm{MeV})\ , \tag{23}$$

the neutron mass cancels, yielding the energy balance equations:

$$\begin{aligned} m[{}^{14}\mathrm{N} + {}^{2}\mathrm{H} - {}^{15}\mathrm{N} - {}^{1}\mathrm{H}]c^2 &= hc/\lambda_1^* \\ m[{}^{12}\mathrm{C} + {}^{2}\mathrm{H} - {}^{13}\mathrm{C} - {}^{1}\mathrm{H}]c^2 &= hc/\lambda_2^* \end{aligned} \tag{24}$$

Thus, precise measurements of the mass differences $^{14}N+^{2}H-^{15}N-^{1}H$ and $^{12}C+^{2}H-^{13}C-^{1}H$ are valuable for γ-ray spectroscopy.

Our best values for these mass differences (Table 5) are accurate to 1×10^{-7} and 4×10^{-7}, respectively. By selecting molecular ions which have optimal correlation among the individual atoms, the final uncertainties in ΔM are minimized. The mass difference $^{14}N+^{2}H-^{15}N-^{1}H$ would be most directly measured from $^{15}NH_3^+/NDH_2^+$, but technical difficulties prevented us from loading ammonia ions into the trap. Instead, the ratios $N_2^+/C_2H_4^+$ and $^{15}N_2^+/C_2D_2H_2^+$ were measured, leading to a value of 9 241 852.1 (1.1) nu for ΔM. As a redundancy check, a value of 9 241 853.7 (1.7) nu was obtained independently from all other ratios ($^{15}N^+/CH_3^+$, N_2^+/CO^+, *etc.*) and is in agreement. The mass difference $^{12}C+^{2}H-^{13}C-^{1}H$ was also measured in two ways to verify its precision. The ratios $^{13}CH_4^+/CDH_3^+$ and $^{13}C_2H_4^+/C_2D_2H_2^+$ determined this difference to be 2 921 907.4 (1.5) nu and 2 921 908.6 (1.2) nu, respectively, and are also in agreement. Our best values for the mass differences, 9 241 852.7 (0.9) nu and 2 921 908.2 (1.1) nu, result from combining these values obtained by independent routes. It is important to note that we have pushed the errors of these critical mass differences down by averaging several runs, with the result that these important ratios have been measured to 5×10^{-11}, an accuracy roughly a factor of two beyond that at which our consistency checks indicate freedom from systematic error. Thus the quoted error depends on our theoretical analysis of systematics.

The previously accepted values of these mass differences from conventional mass spectrometry (36) are also listed in Table 5. Our values for ΔM are about a factor of 10 more accurate than the prior values. The $^{12}C(n, \gamma)$ mass differences are in good agreement; however, the $^{14}N(n, \gamma)$ mass differences do not agree, differing by nine times the reported uncertainty in the prior value. The current γ-ray energy calibration (35) is based on the inconsistent prior value of $^{14}N+^{2}H-^{15}N-^{1}H$. Unlike our redundant Penning trap measurements, the earlier result was based on a single mass comparison. The improved mass difference obtained by Penning trap mass spectrometry considerably increases the accuracy of the energy calibration and suggests that an 8 ppm revision of this calibration is necessary. This is consistent with recent high precision measurements of γ-ray energies with a Ge detector (37).

Table 5. Mass differences for determining α and $N_A h$. The mass differences associated with the neutron capture reactions $^{12}C(n, \gamma)$ and $^{14}N(n, \gamma)$ determined by this experiment and by conventional mass spectrometry (33) are listed. The new results are a factor of 10 more accurate and show considerable discrepancy with the previous value of $^{14}N+^{2}H-^{15}N-^{1}H$.

Mass difference	This work [nu]	Ref. [33] [nu]
$^{14}N+^{2}H-^{15}N-^{1}H$	9 241 852.7 (0.9)	9 241 780 (8)
$^{12}C+^{2}H-^{13}C-^{1}H$	2 921 908.2 (1.1)	2 921 911 (12)

Fundamental constants

A collaboration of researchers using the High Flux Reactor in Grenoble, France is undertaking precision experiments to measure absolute γ-ray wavelengths corresponding to the above reactions ^{14}N(n, γ), ^{12}C(n, γ), and ^{1}H(n, γ) (38). A precision of ~2×10^{-7} is expected for the effective wavelengths λ^* (after taking into account nuclear recoil) corresponding to the mass differences ^{14}N+^{2}H–^{15}N–^{1}H and ^{12}C+^{2}H–^{13}C–^{1}H (39). When this work is completed, the mass differences would not be needed for calibration purposes. Instead, the precise masses and wavelengths could be combined to determine the fundamental constants $N_A h$ and α (40-41).

The molar Planck constant $N_A h$ follows from the fact that the neutron separation energies are measured in different systems of units. We measure the mass defect ΔM in (microscopically defined) atomic mass units (u), while the effective γ-ray wavelength λ^* is measured in S.I. units (m). Equating the energies in Equation (21) leads to:

$$N_A h = \lambda^* \Delta M c \times 10^{-3} \tag{25}$$

where the Avogadro constant $N_A = 10^{-3}\,\Delta M/\Delta m$ is needed to convert ΔM into the mass difference Δm (in kg), required in Equation (21).

Other routes to the accurate determination of $N_A h$ are based on measurements of wavelengths associated with massive particles. The product of the velocity and deBroglie wavelength of a neutron has been measured at the 10^{-7} level (42), and the recoil shift of photons scattered by Cs atoms has been measured at the 10^{-6} level (43). $N_A h$ can determined from either of these measurements combined with measurements of the atomic masses of the respective particles.

The fine structure constant α can also be determined from $N_A h$, and therefore from a measurement of λ^* and ΔM:

$$\alpha^2 = \frac{2R_\infty}{c}\left(\frac{m_p}{m_e}\right)\frac{N_A h}{M_p}\times 10^3 = 2R_\infty\left(\frac{m_p}{m_e}\right)\frac{\Delta M}{M_p}\,\lambda^* \tag{26}$$

The Rydberg constant R_∞, the proton-electron mass ratio m_p/m_e, and the proton atomic mass M_p are known to 4×10^{-11} (44), 3×10^{-9} (45), and 5×10^{-10} (10), respectively. Therefore, measuring λ^* and ΔM with a relative accuracy of ~2×10^{-7} also would determine α to 10^{-7}. Although α has been determined by other experiments with accuracy as high as 10^{-8}, this measurement would be valuable as an independent check and also to verify the consistency of physical theories (46), especially QED, which currently gives the best value of α (47).

ACKNOWLEDGEMENTS

This work was supported by the National Science Foundation (Grant No. PHY-9222768) and the Joint Services Electronics Program (Grant No. DAAL03-92-C-0001). F.D. also acknowledges additional support from an N.S.F. Graduate Fellowship. We are grateful to K. Boyce, E. Cornell, R. Flanagan,

G. Lafyatis, and R. Weisskoff for earlier work on this experiment, and to S. Rusinkiewicz for technical assistance. We also would like to thank M. Matthews for helpful discussions on fitting to the field drift.

REFERENCES

1. F. DiFilippo, V. Natarajan, K.R. Boyce, and D.E. Pritchard, *Phys. Rev. Lett.*. **73**, 1481 (1994).
2. F.M. Penning, *Physica* **3**, 873 (1936).
3. L. Brown and G. Gabrielse, *Rev. Mod. Phys.* **58**, 233 (1986).
4. R.M. Weisskoff *et. al., J. Appl. Phys.* **63**, 4599 (1988).
5. R. Kumaresan and D.W. Tufts, *IEEE Trans. Acous., Speech, and Sig. Proc.* **ASSP-30**, 833 (1982).
6. V. Natarajan, Ph.D. thesis (M.I.T., unpublished, 1993).
7. D.J. Wineland and H.G. Dehmelt, *Int. J. Mass Spec. Ion Proc.* **16**, 338 (1975).
8. E.A. Cornell, R.M. Weisskoff, K.R. Boyce, and D.E. Pritchard, *Phys. Rev. A* **41**, 312 (1990).
9. E.A. Cornell *et. al., Phys. Rev. Lett.* **63**, 1674 (1989).
10. V. Natarajan, K.R. Boyce, F. DiFilippo, and D.E. Pritchard, *Phys. Rev. Lett.* **71**, 1998 (1993).
11. F. DiFilippo, Ph.D. thesis (M.I.T., unpublished, 1994).
12. P.R Bevington and D.K. Robinson, *Data Reduction and Error Analysis for the Physical Sciences*, Second Edition (McGraw-Hill, Inc., New York, 1992).
13. G. Audi and A.H. Wapstra, *Nucl. Phys.* **A565**, 1 (1993).
14. P.J. Huber, *Robust Statistics*, (John Wiley & Sons, New York, 1981).
15. D.F. Andrews *et. al., Robust Estimates of Location: Survey and Advances*, (Princeton University Press, Princeton, NJ, 1972).
16. S.G. Lias *et. al., J. Phys. Chem. Ref. Data* **17**, Suppl. 1 (1988).
17. A.H. Wapstra and G. Audi, *Nucl. Phys.* **A432**, 1 (1985).
18. G.L. Greene, E.G. Kessler, Jr., R.D. Deslattes, and H. Börner, *Phys. Rev. Lett.* **56**, 819 (1986).
19. R.S. Van Dyck, Jr., D.L. Farnham, and P.B. Schwinberg, *J. Mod. Opt.* **39**, 243 (1992).
20. R.S. Van Dyck, Jr., D.L. Farnham, and P.B. Schwinberg, *Phys. Rev. Lett.* **70**, 2888 (1993).
21. R. Jertz *et. al., Physica Scripta* **48**, 399 (1993).
22. H.-J. Kluge, *Phys. Scrip.* **T22**, 85 (1988).
23. M. Comisarow and A. Marshall, *Int. J. Mass Spect. Ion Proc.* **118** 37 (1992).
24. M.V. Gorshkov *et. al., J. Am. Soc. Mass Spec.* **4**, 855 (1993).
25. M.V. Gorshkov *et. al., Phys. Rev. A* **47**, 3433 (1993).
26. M.V. Gorshkov *et. al., Int. J. Mass Spec. Ion Proc.* **128**, 47 (1993).
27. E.A. Cornell, K.R. Boyce, D.L.K. Fygenson, and D.E. Pritchard, *Phys. Rev. A* **45**, 3049 (1992).
28. F. DiFilippo, V. Natarajan, K.R. Boyce, and D.E. Pritchard, *Phys. Rev. Lett.* **68**, 2859 (1992).
29. V. Natarajan, F. DiFilippo, and D.E. Pritchard, to be published.
30. V. Natarajan, K.R. Boyce, F. DiFilippo, and D.E. Pritchard, in *Nuclei Far From Stability / Atomic Masses and Fundamental Constants 1992*, R. Neugart and A. Wöhr, Eds., p. 13 (1992).
31. T.J. Quinn, *IEEE Trans. Instr. Meas.* **40**, 81 (1991).
32. B.N. Taylor, *IEEE Trans. Instr. Meas.* **40**, 86 (1991).
34. P. Seyfried *et. al., Z. Phys. B* **87**, 289 (1992).
34. G. Basile *et. al., Phys. Rev. Lett.* **72**, 3133 (1994).
35. A.H. Wapstra, *Nucl. Instr. Meth. Phys. Res.* **A292**, 671 (1990).
36. L.G. Smith and A.H. Wapstra, *Phys. Rev. C* **11**, 1392 (1975).

37. S. Raman, private communication.
38. M.S. Dewey *et. al.*, *Nucl. Instr. Meth. Phys. Res.* **A284**, 151 (1989).
39. G.L. Greene and E.G. Kessler, Jr., private communications.
40. R.D. Deslattes and E.G. Kessler, Jr., in *Atomic Masses and Fundamental Constants – 6*, J.A. Nolen, Jr. and W. Benenson, Eds., (Plenum Press, New York, 1979), p. 203.
41. W.H. Johnson, in *Precision Measurements and Fundamental Constants II*, B.N. Taylor and W.D. Phillips, Eds., Natl. Bur. Stand. (U.S.), Spec. Publ. 617 (U.S. GPO, Washington D.C., 1984), p. 335.
42. E. Krüger, W. Nistler, and Weirauch, "Determination of the fine-structure constant by measuring the quotient of the Planck constant and the neutron mass" presented at the Conference on Precision Electromagnetic Measurements, Boulder CO, June 27 - July 1 (1994).
43. D. S. Weiss, B. C. Young, and S. Chu, *Phys. Rev. Lett* **70**, 2706 (1993).
44. T. Andreae *et. al.*, *Phys. Rev. Lett.* **69**, 1923 (1992).
45. R. S. Van Dyck, Jr., D. L. Farnham, and P. B. Schwinberg, "Proton/ electron mass ratio and the electron's 'atomic mass'", presented at the Conference on Precision Electromagnetic Measurements, Boulder CO, June 27 - July 1 (1994).
46. G.L. Greene, M.S. Dewey, E.G. Kessler, Jr., and E. Fischbach, *Phys. Rev. D* **44**, R2216 (1991).
47. T. Kinoshita, *Metrologia* **25**, 233 (1988).